

This discussion paper is/has been under review for the journal Atmospheric Chemistry and Physics (ACP). Please refer to the corresponding final paper in ACP if available.

Radical mechanisms of methyl vinyl ketone oligomerization through aqueous phase OH-oxidation: on the paradoxical role of dissolved molecular oxygen

P. Renard¹, F. Siekmann¹, A. Gandolfo¹, J. Socorro¹, G. Salque³, S. Ravier¹, E. Quivet¹, J.-L. Clément², M. Traikia⁵, A.-M. Delort^{5,6}, D. Voisin³, R. Thissen⁴, and A. Monod¹

¹Aix-Marseille Université, CNRS, LCE FRE 3416, 13331 Marseille, France

²Aix-Marseille Université, CNRS, ICR UMR 7273, 13397 Marseille, France

³Université Joseph Fourier, Grenoble 1/CNRS-INSU, Laboratoire de Glaciologie et Géophysique de l'Environnement, 54 rue Molière, 38402 Saint-Martin-d'Hères, France

⁴Institut de Planétologie et d'Astrophysique de Grenoble (IPAG) UMR5274, UJF-Grenoble1/CNRS-INSU, Grenoble, 38041, France

⁵Clermont Université, Université Blaise Pascal, Institut de Chimie de Clermont-Ferrand, BP 10448, 63000 Clermont-Ferrand, France

⁶CNRS, UMR 6296, ICCF, BP 80026, 63171 Aubière, France

2913

Received: 17 December 2012 – Accepted: 3 January 2013 – Published: 28 January 2013

Correspondence to: P. Renard (renard.pascal@yahoo.fr), A. Monod (anne.monod@univ-amu.fr)

Published by Copernicus Publications on behalf of the European Geosciences Union.

Abstract

It is now accepted that one of the important pathways of Secondary Organic Aerosol (SOA) formation occurs through aqueous phase chemistry in the atmosphere. However, the liquid phase chemical mechanisms leading to macromolecules are still not well understood. For α -dicarbonyl precursors, such as methylglyoxal and glyoxal, radical reactions through OH-oxidation produce oligomers, irreversibly and faster than accretion reactions. Methyl vinyl ketone (MVK) was chosen in the present study as it is an α , β -unsaturated carbonyl that can undergo such reaction pathways in the aqueous phase and forms even high molecular weight oligomers. We present here experiments on the aqueous phase OH-oxidation of MVK, performed under atmospheric relevant conditions. Using NMR and UV absorption spectroscopy, high and ultra-high resolution mass spectrometry, we show that the fast formation of oligomers up to 1800 Da is due to radical oligomerization of MVK, and 13 series of oligomers (out of a total of 26 series) are identified. The influence of atmospherically relevant parameters such as temperature, initial concentrations of MVK and dissolved oxygen are presented and discussed. In agreement with the experimental observations, we propose a chemical mechanism of OH-oxidation of MVK in the aqueous phase that proceeds via radical oligomerization of MVK on the olefin part of the molecule. This mechanism highlights the paradoxical role of dissolved O_2 : while it inhibits oligomerization reactions, it contributes to produce oligomerization initiator radicals, which rapidly consume O_2 , thus leading to the supremacy of oligomerization reactions after several minutes of reaction. These processes, together with the large ranges of initial concentrations investigated (60–656 μ M of dissolved O_2 and 0.2–20 mM of MVK) show the fundamental role that O_2 likely plays in atmospheric organic aerosol.

2915

1 Introduction

Although Secondary Organic Aerosol (SOA) represents a substantial part of organic aerosol, which affects air quality, climate and human health, the understanding of its formation pathways and its properties is still limited due to the complexity of the physicochemical processes involved. It is now accepted that one of the important pathways of SOA formation occurs through aqueous phase chemistry which is a favorable medium for the formation of oligomers (Hallquist et al., 2009; Carlton et al., 2009; Ervens et al., 2011). An oligomer is a molecule that consists of a few monomer units (roughly up to 30). Such aqueous phase chemistry is obviously relevant to clouds and fogs, but not limited to them, by far: it was shown that water can make up most of the aerosol mass, and in many cases largely exceeds the sum of all other particle species including organic matter (Tan et al., 2012; Liao and Seinfeld, 2005). This actually extends the relevance of aqueous phase processes from water vapor supersaturated regions of the atmosphere to high relative humidity regions, which represents a high fraction of the atmosphere. However, the aqueous phase chemical mechanisms leading to oligomers or macromolecules such as HULIS are still not well understood. Several accretion mechanisms such as aldol condensation, acetal formation or esterification have been tentatively proposed, but it was recently recognized that aqueous phase photochemistry plays a crucial role in oligomer development. For α -dicarbonyl precursors, such as methylglyoxal (Tan et al., 2012) and glyoxal (Lim et al., 2010), radical reactions through OH-oxidation produce oligomers, irreversibly and faster than accretion reactions.

Recent studies showed that aerosol water-soluble organic carbon (WSOC) is a complex mixture that contains thousands of organic compounds among which a majority is aliphatic to olefinic in nature, and indicate significant non-oxidative reaction pathways for the formation of high molecular weight WSOC components (Mazzoleni et al., 2012). Methyl vinyl ketone (MVK) was chosen for the present study as it is an α , β -unsaturated carbonyl that can possibly undergo such non-oxidative reaction pathways in the aqueous phase, as it was preliminarily shown by Liu et al. (2012).

2916

The aim of the present study is to determine the radical mechanism involved in the oligomerization of MVK, and to identify the oligomers formed via this chemistry. The influence of atmospherically relevant parameters such as temperature, reactant initial concentrations and dissolved oxygen concentrations is studied.

5 2 Experimental

We used a photoreactor to simulate the aqueous phase photooxidation of MVK under atmospheric conditions. HO[•] radicals were generated from H₂O₂ photolysis. In order to determine the reaction mechanism, we used a complete set of analytical strategies to identify the oligomers produced. Aqueous aliquots sampled at different photoreaction times were analyzed by mass spectrometry, UV absorbance spectroscopy and NMR. In order to test our radical mechanism for MVK oligomerization, its aqueous phase photooxidation was studied under various relevant conditions of temperature, MVK initial concentrations, and above all, dissolved oxygen concentrations.

2.1 Photoreactor

The photoreactor set-up we used is based on the one described by Liu et al. (2009, 2012) with some modifications. It is a 450 cm³ Pyrex thermostated photoreactor. The arc light source (LSH 601, Lot Oriel) is equipped with a 1000 W xenon arc lamp (LSB 551, Lot Oriel). A glass filter (ASTM 892 AM 1.5 standard) was used to remove the UV irradiation below 300 nm, resulting in an irradiance spectrum comparable to that of the sun at sea level, for a 48.3° zenith angle, but more intense (less than an order of magnitude).

Compared to the set-up used by Liu et al. (2009, 2012), the photolysis rate constant of H₂O₂ increased by an order of magnitude due to the more powerful lamp used (Table 1). This resulted in higher HO[•] concentrations using lower H₂O₂ initial

2917

concentrations, and thus led to faster MVK degradation and kept artifacts due to H₂O₂ reactivity to a minimum.

A 50 mL gas space was left over the liquid level. The loss of aqueous MVK to the gas phase was insignificant, based on its Henry's Law constant (41 Matm⁻¹ at 25 °C; Iraci et al., 1999) and on control experiments.

2.2 Experimental conditions

All experiments started with irradiation of UHQ water (18.2 Mohmcm, Millipore), then H₂O₂ (30%, non-stabilized, Acros) was introduced, photolysed for 10 min until photo-stationary conditions were reached. MVK (99%, Sigma Aldrich) was finally introduced at time noted 0 min. The experimental conditions (temperature, concentrations) were chosen in order to be representative of cloud droplets or deliquesced aerosol particles conditions.

2.2.1 Control experiments

To check that the observed products resulted from the aqueous phase OH-oxidation of MVK, two control experiments were conducted: (1) MVK (20 mM) + H₂O₂ (400 mM) under dark conditions, and (2) direct photolysis of MVK (20 mM). MVK was not significantly consumed either in presence of H₂O₂ in the dark (1) or under direct irradiation (2). Additionally, we performed (3) direct photolysis of H₂O₂ (400 mM) in absence of MVK, and the observed decrease of H₂O₂ concentrations allowed us to determine its photolysis rate constant *J* (see Table S1 in the Supplement). The duration of these three control experiments was 300 min, consistent with the reaction time of the actual MVK photooxidation experiments.

2.2.2 Initial concentrations of reactants

Tan et al. (2010) have shown the important impact of initial concentrations on oligomer formation for α -dicarbonyls. Our experiments were thus carried out with various

2918

patterns. Typical standard deviation of the Kendrick mass defect in any such identified series was lower than 0.5 mDa which ensures the proper attribution of all the members of a series, to within less than 1 mDa in the full mass range explored (i.e. 50–1500 Da).

2.4 Spectroscopic analyses of the solution

2.4.1 UV Spectroscopy

UV absorption spectroscopy (Agilent 8453) was used in a wavelength range from 190 to 400 nm to monitor MVK concentrations and chemical structure changes during the reaction. Diluted in water, MVK shows, like all α,β -unsaturated ketones (Yadav, 2012), an intense absorption band (K-band; $\pi \rightarrow \pi^*$ transition) at 211 nm ($\epsilon_{211} = 7692 \text{ M}^{-1} \text{ cm}^{-1}$) and a weak absorption band (R-band; $n \rightarrow \pi^*$ transition) at 296 nm ($\epsilon_{296} = 30 \text{ M}^{-1} \text{ cm}^{-1}$). Because the absorbance of H_2O_2 below 240 nm is intense (i.e. $\epsilon_{211} = 100 \text{ M}^{-1} \text{ cm}^{-1}$), it was interfering with the $\pi \rightarrow \pi^*$ transition of MVK under our experimental conditions where $[\text{H}_2\text{O}_2]_0/[\text{MVK}]_0=20$. A volume of catalase from bovine liver (C 3155, Sigma Aldrich) was added to each sample to quench efficiently the H_2O_2 absorbance signal within a few minutes (Li and Schellhorn, 2007).

2.4.2 NMR spectroscopy

One of the experiments A was analyzed using NMR spectroscopy (Table 1). The instrument used was a Bruker Avance 500 MHz equipped with a 5 mm inverse-triple tuned (TXI) $^1\text{H}/^{13}\text{C}/^{15}\text{N}$ with z-gradient coil probe. For 1-D ^1H -Spectra, 128 scans were collected with an impulsion time of 7.5 μs , a relaxation delay of 5 s, an acquisition time of 4.67 s, a spectral window of 5000 Hz and 64 K data points zero-filled to 128 K before Fourier transformation with 0.3 Hz line broadening. For 2-D homonuclear (COSY and TOCSY) and heteronuclear ($^1\text{H}/^{13}\text{C}$ HSQC and HMBC) experiments were performed with quadrature phase detection in both dimensions, using state-TPPI or QF detection mode in the indirect one. For each 256 (homonuclear experiments) or

2923

512 (heteronuclear experiments) increments in the indirect dimension, 2K data points were collected and 16 or 32 transients were accumulated in the direct dimension. ^{13}C decoupling (GARP) was performed during acquisition time for heteronuclear experiments. A $\pi/2$ shifted square sine-bell function was applied in the indirect dimension before Fourier transformation. Spectra were treated with Topspin version 2.0. All NMR spectra were recorded at 25 $^\circ\text{C}$.

Aliquots of 540 μL of the aqueous solution sampled from the photoreactor (at 5, 10, 25, 70 and 90 min of reaction) was supplemented with 60 μL of a buffer containing 100 mM phosphate and 5 mM of sodium tetra deuterated trimethylsilyl propionate (TSPd₄, Eurisotop). TSPd₄ constituted a reference for chemical shifts (0 ppm) and quantification. Final volumes of 600 μL of prepared samples were put in 5 mm-diameter NMR tubes.

Additionally, an aliquot of 5 mL sampled at the end of the kinetic (90 min of reaction) was freeze-dried, re-suspended in 600 μL of CDCl_3 and transferred in a 5 mm NMR tube for further 1-D and 2-D NMR analysis. D_2O and CDCl_3 were used for locking and shimming.

3 Results and discussions

3.1 Evidence for the formation of oligomers by radical oligomerization of MVK

The aqueous phase OH-oxidation of MVK leads to the formation of series of oligomers as indicated by the analytical devices used, and is in good agreement with the study by Liu et al. (2012). Furthermore, the whole set of analyses showed that the produced oligomers were formed by radical oligomerization of MVK, as discussed below. The ionic oligomerization of MVK (through carbocations or carbanions) was unlikely under our experimental conditions because the protic and nucleophilic characters of the solvent (water) inhibit oligomerization by reacting instantly with carbocation and carbanion initiators (Odian, 2004).

2924

3.1.1 Series of oligomers evidenced by mass spectrometry and NMR spectroscopy

Figure 1 shows a mass spectrum (obtained using UPLC-ESI-MS) for the retention time range 0–7 min, recorded in the positive mode, at 50 min of MVK photooxidation at 5 °C (experiment C in Table 1). Spectra typically contain hundreds of peaks in both modes, and it was out of the scope of this study to explore their full complexity. Yet, oligomer systems are clearly visible, with very regular spacing of 70.0419 Da, which correspond to the exact mass of the precursor, MVK, as confirmed by the ESI-UHRMS analysis. These systems extend up to 1800 Da, thus containing up to 25 monomers. Using a lower intensity xenon lamp, and a lower resolution mass spectrometer (Table 1), Liu et al. (2012) also found oligomer series at the same nominal masses, with slightly different intensities. The main differences observed here were the kinetics. The maximum intensity was reached around 50 min here at 25 °C, instead of 20 h previously (Liu et al., 2012) at the same temperature, certainly due to the higher HO[•] concentrations obtained here with a more powerful irradiation lamp (Table 1).

Experiment A was repeated 12 times and analyzed using the same UPLC-ESI-MS conditions. The exact masses measured for the oligomers were very repeatable, as was the kinetics of their appearance and of MVK consumption.

Experiment A was also monitored once using ¹H NMR spectroscopy (Table 1). Figure 2 shows ¹H NMR peaks resonating at 2.36 ppm (s), 6.13 ppm (dd), 6.37 ppm (m) and 6.39 ppm (m) that were assigned to the ¹H of MVK. These ¹H peaks decreased with time while new ¹H NMR signals resonating at 1.15–1.88 ppm and 2.13–2.34 ppm increased with time, indicating the formation of reaction products, to the detriment of MVK. These signals are very wide and are consistent with the presence of overlapping signals due to a variety of oligomers. Overall, both mass spectrometry and NMR measurements indicate that a wide variety of oligomers was formed from the reactivity of MVK and that this formation of high mass oligomers occurs through an extremely fast mechanism, as in radical propagation systems.

2925

3.1.2 Indications on the chemical structure of the monomers according to NMR and UV-spectroscopic measurements

In order to identify the structure of the oligomers observed by ¹H NMR spectroscopy in Fig. 2, the sample taken at the end of the reaction (experiment A at 90 min) was freeze-dried and re-suspended in CDCl₃ leading to a concentrated solution of the oligomers allowing the measurement of 1-D and 2-D NMR spectra (Fig. 3). The analysis of the ¹H NMR resonances in the 1-D ¹H NMR spectrum (Fig. 3a) and of the ¹J_{1H-13C} correlations present on the 2D ¹H–¹³C HSQC NMR spectrum (Fig. 3b) allowed proposing assignments of CH, CH₂ and CH₃ functional groups of the putative oligomeric structure shown in Fig. 3. Long range J_{1H-13C} correlations observed on the 2-D ¹H–¹³C HMQC NMR spectrum (Fig. 3c) clearly demonstrated the presence of C=O functional groups belonging to the proposed oligomeric structure. NMR experiments also showed that MVK was largely converted into oligomer forms and that most of the signals of C=C bonds have disappeared at 70 and 90 min of reaction, thus indicating that the oligomers are mostly aliphatic.

Using UV absorption spectroscopy from 190 to 400 nm during experiment A, the evolution of the two intense absorption bands of MVK are shown in Fig. 4. During the photooxidation process, the *n* → *π*^{*} transition (Fig. 4a) was clearly shifted to shorter wavelengths (blue shift; i.e. from 296 nm at time 0 to 269 nm at 90 min of reaction), with increasing absorption intensity. The *π* → *π*^{*} transition did not show any shift (in the range of the investigated wavelengths) (Fig. 4b), but a clear decrease of its intensity (at 211 nm) was observed. The observed blue shift shows that, in the reaction products formed, the corresponding transition needs higher energy (than in MVK) to get excited (i.e. at shorter wavelengths). This can be due to the loss of the conjugation, probably due to the loss of the vinyl function, in good agreement with the NMR analyses. Furthermore, the absorption intensity at 211 nm was directly proportional to the MVK concentrations during the reaction, as we verified with ¹H NMR (at 2.36 ppm) and with mass spectrometry.

2926

3.3.2 Effects of initial concentrations of dissolved oxygen and temperature

Experiments A and D (Table 1) were performed under the same initial concentrations of MVK (20 mM) and temperature (25 °C), with very different initial dissolved O₂ concentrations: supersaturated and low initial O₂ concentrations, respectively, i.e. higher and lower than Henry's law equilibrium (by a factor of 1.7 and 4.5, respectively; Table 1). The results showed that the initial dissolved O₂ concentrations had a drastic effect on oligomerization, and on the kinetics of MVK consumption, in very good agreement with a mechanism of radical oligomerization of MVK. Dissolved O₂ is known to inhibit free radical photo-oligomerization by reacting with radical species to form chain terminating oxygenated compounds such as hydroperoxides (Decker and Jenkins, 1985). In our experiments, a clear inhibition of the oligomer formation by dissolved O₂ was observed (Fig. 8a): at low initial O₂ concentrations (experiment D), the whole oligomer series developed within 5 min of reaction, while only first elements of the series appeared at the same reaction time under "supersaturated initial O₂ concentrations" (experiment A). This phenomenon, which was observed for all the other series of oligomers, shows that the reactivity of the initiator radicals (iR^{*}) underwent a competition kinetic between their reaction towards O₂ and towards MVK for further oligomerization propagation. When O₂ was present, iR^{*} consumed O₂ very rapidly (i.e. faster than O₂ renewal from the gas phase and from H₂O₂ reactivity), and when O₂ concentration was sufficiently low, the competition furthered the oligomerization pathway which was extremely fast. Figure 9 shows a very contrasting behavior of MVK time profiles between "low initial O₂ concentrations" and "supersaturated initial O₂ concentrations" conditions. Under "supersaturated initial O₂ concentrations", two kinetic steps were observed: a slow one during which the oligomers were poorly formed, followed by a fast one where oligomers were actively formed (Figs. 5 and 9b). In contrast, under "low initial O₂ concentrations", the kinetic of MVK consumption was fast from the beginning (only one step was observed), and oligomerization started as soon as MVK was introduced (Figs. 9a and 8).

2931

Figure 9 also shows the behavior of dissolved O₂ under three different conditions (experiments D, A and C). For all of these conditions, before the injection of H₂O₂, dissolved O₂ was at its Henry's law equilibrium with ambient O₂ in the gas phase. When H₂O₂ was added, dissolved O₂ concentrations increased due to the self-reaction of HO₂^{*} and/or O₂^{*-} radicals in the aqueous phase (see reactions R3 and R4 in the Supplement). Then, as soon as MVK was introduced, the time profiles of O₂ concentration followed those of MVK, thus indicating that O₂ reacted with the radicals formed from MVK, even when oligomerization was the dominant pathway. Interestingly, under "supersaturated initial O₂ concentrations", the oligomerization acceleration started when O₂ concentrations were depleted from their initial values, but still they were higher than their Henry's law equilibrium (by a factor of 1.2 and 1.4 at 25 and 5 °C, respectively), thus showing the atmospheric relevance of these oligomerization processes.

Experiments A, B and C differ for the temperature (i.e., 25 °C, 9 °C and 5 °C) with identical initial concentrations of MVK (20 mM) and similar dissolved O₂ concentration (supersaturated). The kinetic decay of MVK was clearly influenced by the temperature during the initial step (Fig. 9b, c). Additionally, the lower temperature induced higher initial dissolved O₂ concentrations, and both these phenomena explain the time delay of the acceleration of oligomerization at 5 °C compared to 25 °C (at around 25 and 13 min, respectively). In contrast, the fast decay of MVK was not influenced by the temperature, thus showing that the radical mechanism of oligomerization of MVK at 20 mM is the dominant pathway for MVK consumption at this step.

Finally, when most of the MVK was consumed, all oligomer series reached their maximum intensities, with slight differences from one condition to the other as illustrated for one series in Fig. 8b. These differences are particularly interesting to investigate the comprehension of the initial steps of the radical mechanism.

3.4 Identification of oligomers and their initiator radicals

In Fig. 10, starting from the known mechanism of OH-oxidation of MVK in the aqueous phase (Liu, 2011; Zhang et al., 2010), we added the possible oligomerization

2932

In this mechanism, the formed low-molecular-weight compounds (LMWC, such as formaldehyde, methylglyoxal, glyoxal, oxalic, formic, pyruvic, malonic and acetic acids, observed by Zhang et al., 2010 during the OH-oxidation of MVK under similar conditions) can also further react with HO[•] and produce other iR[•] radicals, which can oligomerize. However, the corresponding oligomers were observed here only for acetic acid and methylglyoxal, which were among the major low-molecular-weight products observed by Zhang et al. (2010). A confirmation of these observations was brought by two extra experiments (A' and A'') where 2 mM of methylglyoxal and acetic acid (Sigma Aldrich), respectively, were injected in the vessel at the same time as MVK injection. The results showed a significant increase (by 42 % and 77 %, respectively) of the corresponding oligomer series (S140' and S142 and series S128 and S130, respectively), compared to experiment A. Furthermore, experiment C (performed at 5 °C) allowed us to clearly observe the kinetics of oligomer formation (Fig. 11). The series R-(MVK)_n (S156) were directly formed, immediately followed by the series R-(MVK)_n-OOH (S190) (which require O₂ addition), and the series (Methylglyoxal)-(MVK)_n (S142) and (Acetic acid)-(MVK)_n (S130) were formed later, in very good agreement with the proposed mechanism (in Fig. 10).

The role of molecular O₂ was evidenced by the intensities of the identified series (Table 2). Comparing experiments A and D (i.e. from supersaturated to low initial O₂ conditions, respectively), after 50 min of reaction, we observed a systematic increase of the intensities of all series not requiring O₂ addition, and a systematic decrease of those requiring O₂ addition. This observation is also in very good agreement with the proposed mechanism (Fig. 10) described above, and it shows the prevailing role of oxygen on the processes.

4 Conclusions

This paper reports on an experimental study of the aqueous phase OH-oxidation of methyl vinyl ketone, under atmospheric conditions of clouds or deliquesced aerosol

2935

particles. In good agreement with Liu et al. (2012), we showed that this reactivity leads to the formation of oligomers via a radical oligomerization mechanism. Using mass spectrometry, 26 series of oligomers were detected with highly regular patterns of mass differences of 70.0419 Da (corresponding to the molecular mass of MVK) up to 1800 Da, in both positive and negative modes. Additionally, the kinetics of the reactions, monitored by NMR and UV spectroscopy, indicated that MVK was largely converted into oligomeric forms with the decrease of the olefin structures, correlated with the increase of aliphatic carbonyl oligomers. Using high and ultra-high resolution mass spectrometry, the elemental composition of 13 series of oligomers was determined.

The investigation of the influence of key parameters, i.e. temperature, initial MVK concentrations and initial dissolved O₂ concentrations showed important impacts on the oligomerization process. The mass of oligomers increased with the initial MVK concentrations. Under supersaturated initial O₂ concentrations, the initiation of oligomerization was delayed compared to low initial O₂ concentrations, and this delay increased with decreasing temperature.

In agreement with the experimental observations, we proposed a complete radical mechanism of OH-oxidation of MVK in the aqueous phase proceeding via oligomerization of MVK by opening its carbon-carbon double bond, initiated from several initiator organic radicals (iR[•]). Among the latter were those directly formed by OH-oxidation of MVK, and also those formed from the OH-oxidation of MVK's main oxidation products, e.g. acetic acid and methylglyoxal. The proposed mechanism allowed for explaining the particular role of dissolved O₂ under our experimental conditions. Each iR[•] radical underwent competition kinetics between O₂ addition (Reaction R1) and oligomerization (Reaction R2):



Supersaturated initial O₂ concentrations inhibited radical oligomerization by fast addition on iR[•] resulting in the formation of LMWC (such as acetic acid and methylglyoxal),

2936

which were further OH-oxidized and formed other iR^{\bullet} radicals. The fast O_2 addition reactions resulted in a fast decrease of O_2 concentrations in the vessel, faster than O_2 renewal from the gas phase and from the reactivity of H_2O_2 , and even faster than MVK consumption. At initial MVK concentrations higher than 0.2 mM, the decrease of O_2 concentrations resulted in the dominance of reaction (2) after several minutes, and oligomerization started, even when O_2 concentrations were still higher than Henry's law equilibrium with atmospheric O_2 . The paradoxical role of O_2 resides in the fact that while it inhibits oligomerization, it produces more iR^{\bullet} radicals, which contribute to O_2 consumption, and thus lead to oligomerization. These processes, together with the large ranges of initial concentrations investigated (60–656 μM of dissolved O_2 and 0.2–20 mM of MVK concentrations) show the fundamental role that O_2 likely plays in atmospheric aerosols. Further studies are needed to investigate the actual ranges of O_2 concentrations in the condensed phases in order to assert the importance of the oligomerization processes established here in the atmosphere.

In the proposed mechanism, some ubiquitous radicals in the atmospheric aqueous phase (such as those resulting from the reactivity of acetic acid and methylglyoxal) can be very efficient initiator radicals. The latter radicals simply require sufficiently concentrated olefins to initiate oligomerization with fast propagation and prompt growth of the chain, resulting in the formation of very high molecular weight compounds. It is thus of high interest to investigate the potential concentrations of olefin structures in the condensed phase of the atmosphere.

In the proposed mechanism, oligomerization mechanisms proceed via non-oxidative pathways. Such pathways in the aqueous phase can explain some atmospheric observations such as those of Mazzoleni et al. (2012) who investigated elemental composition of WSOC by ultra-high resolution mass spectrometry. Their results indicated significant non-oxidative reaction pathways for the formation of high molecular weight WSOC components in organic aerosols sampled during summer in a rural site where SOA was abundant.

2937

Supplementary material related to this article is available online at:
<http://www.atmos-chem-phys-discuss.net/13/2913/2013/acpd-13-2913-2013-supplement.pdf>.

Acknowledgements. We thank the National Research Agency ANR (project Cumulus), AXA insurances and CNRS-INSU for funding this research. We also thank Barbara Ervens (CIRES, University of Colorado, Boulder and Chemical Sciences Division, National Oceanic and Atmospheric Administration (NOAA), Boulder, CO, USA) and Gaëlle Gosset (Aix-Marseille Université, CNRS, ICR UMR 7273, 13397, Marseille, France) for valuable scientific discussions on this topic.

References

- Bateman, A. P., Walser, M. L., Desyaterik, Y., Laskin, J., Laskin, A., and Nizkorodov, S. A.: The effect of solvent on the analysis of secondary organic aerosol using electrospray ionization mass spectrometry, *Environ. Sci. Technol.*, 42, 7341–7346, doi:10.1021/es801226w, 2008.
- Benson, B. B. and Krause, D.: The concentration and isotopic fractionation of oxygen dissolved in freshwater and seawater in equilibrium with the atmosphere, American Society of Limnology and Oceanography Inc., Department of Physics, Amherst College, Amherst, Massachusetts, USA, 1984.
- Carlton, A. G., Wiedinmyer, C., and Kroll, J. H.: A review of Secondary Organic Aerosol (SOA) formation from isoprene, *Atmos. Chem. Phys.*, 9, 4987–5005, doi:10.5194/acp-9-4987-2009, 2009.
- Danger, G., Orthaus-Daunay, F. R., de Marcellus, P., Modica, P., Vuitton, V., Duvernay, F., Flandinet, L., Le Sergeant d'Hendecourt, L., Thissen, R., and Chiavassa, T.: Characterization of laboratory analogs of interstellar/cometary organic residues using very high resolution mass spectrometry, *Geochim. Cosmochim. Acta*, submitted, 2013.
- Decesari, S., Facchini, M. C., Fuzzi, S., McFiggans, G. B., Coe, H., and Bower, K. N.: The water-soluble organic component of size-segregated aerosol, cloud water and wet depositions from Jeju Island during ACE-Asia, *Atmos. Environ.*, 39, 211–222, 2005.

2938

- Decker, C. and Jenkins A. D.: Kinetic approach of O₂ inhibition in ultraviolet- and laser-induced polymerizations, *Macromolecules*, 18, 1241, doi: 10.1021/ma00148a034, 1985.
- Ervens, B. and Volkamer, R.: Glyoxal processing by aerosol multiphase chemistry: towards a kinetic modeling framework of secondary organic aerosol formation in aqueous particles, *Atmos. Chem. Phys.*, 10, 8219–8244, doi:10.5194/acp-10-8219-2010, 2010.
- Ervens, B., Turpin, B. J., and Weber, R. J.: Secondary organic aerosol formation in cloud droplets and aqueous particles (aqSOA): a review of laboratory, field and model studies, *Atmos. Chem. Phys.*, 11, 11069–11102, doi:10.5194/acp-11-11069-2011, 2011.
- Gibian, M. J. and Corley, R. C.: Organic radical-radical reactions. Disproportionation vs. combination, *Chem. Rev.*, 73, 441–464, doi:10.1021/cr60285a002, 1973.
- Hallquist, M., Wenger, J. C., Baltensperger, U., Rudich, Y., Simpson, D., Claeys, M., Dommen, J., Donahue, N. M., George, C., Goldstein, A. H., Hamilton, J. F., Herrmann, H., Hoffmann, T., Iinuma, Y., Jang, M., Jenkin, M. E., Jimenez, J. L., Kiendler-Scharr, A., Maenhaut, W., McFiggans, G., Mentel, Th. F., Monod, A., Prévôt, A. S. H., Seinfeld, J. H., Surratt, J. D., Szmigielski, R., and Wildt, J.: The formation, properties and impact of secondary organic aerosol: current and emerging issues, *Atmos. Chem. Phys.*, 9, 5155–5236, doi:10.5194/acp-9-5155-2009, 2009.
- Hennigan, C. J., Bergin, M. H., Russell, A. G., Nenes, A., and Weber, R. J.: Gas/particle partitioning of water-soluble organic aerosol in Atlanta, *Atmos. Chem. Phys.*, 9, 3613–3628, doi:10.5194/acp-9-3613-2009, 2009.
- Herrmann, H., Hoffmann, D., Schaefer, T., Brüner, P., and Tilgner, A.: Tropospheric aqueous phase free radical chemistry: radical sources, spectra, reaction kinetics and prediction tools, *Chem. Phys. Phys. Chem.*, 11, 3796–3822, 2010.
- Hobby, K.: A novel method of isotope prediction applied to elemental composition analysis, Micromass MS Technologies, Floats Road, Manchester, M23 9LZ, UK, Waters Corporation, 2005.
- Huang, D., Zhang, X., Chen, Z. M., Zhao, Y., and Shen, X. L.: The kinetics and mechanism of an aqueous phase isoprene reaction with hydroxyl radical, *Atmos. Chem. Phys.*, 11, 7399–7415, doi:10.5194/acp-11-7399-2011, 2011.
- Hughey, C. A., Hendrickson, C. L., Rodgers, R. P., and Marshall, A. G.: Kendrick mass defect spectrum: a compact visual analysis for ultrahigh-resolution broadband mass spectra, *Anal. Chem.*, 73, 4676–4681, 2001.

2939

- Iraci, L. T., Baker, B. M., Tyndall, G. S., and Orlando, J. J.: Measurements of the Henry's law coefficients of 2-methyl-3-buten-2-ol, methacrolein, and methyl vinyl ketone, *J. Atmos. Chem.*, 33, 321–330, 1999.
- Li, Y. and Schellhorn, H. E.: Rapid kinetic microassay for catalase activity, *J. Biomol. Tech.*, 18, 185–187, 2007.
- Lim, Y. B., Tan, Y., Perri, M. J., Seitzinger, S. P., and Turpin, B. J.: Aqueous chemistry and its role in secondary organic aerosol (SOA) formation, *Atmos. Chem. Phys.*, 10, 10521–10539, doi:10.5194/acp-10-10521-2010, 2010.
- Liu, Y.: Etudes des impacts de la réactivité en phase aqueuse atmosphérique sur la formation et le vieillissement des Aérosols Organiques Secondaires sous conditions simulées, Ph. D. thesis, Laboratoire de Chimie de l'Environnement, Aix-Marseille University, Marseille, France, 2011.
- Liu, Y., El Haddad, I., Scarfogliero, M., Nieto-Gligorovski, L., Temime-Roussel, B., Quivet, E., Marchand, N., Picquet-Varrault, B., and Monod, A.: In-cloud processes of methacrolein under simulated conditions – Part 1: Aqueous phase photooxidation, *Atmos. Chem. Phys.*, 9, 5093–5105, doi:10.5194/acp-9-5093-2009, 2009.
- Liu, Y., Siekmann, F., Renard, P., El Zein, A., Salque, G., El Haddad, I., Temime-Roussel, B., Voisin, D., Thissen, R., and Monod, A.: Oligomer and SOA formation through aqueous phase photooxidation of methacrolein and methyl vinyl ketone, *Atmos. Environ.*, 49, 123–129, doi:10.1016/j.atmosenv.2011.12.012, 2012.
- Makarov, A., Denisov, E., Lange, O. and Horning, S.: Dynamic range of mass accuracy in LTQ orbitrap hybrid mass spectrometer, *J. Am. Soc. Mass Spectr.*, 17, 977–982, doi:10.1016/j.jasms.2006.03.006, 2006.
- Mazzoleni, L. R., Saranjampour, P., Dalbec, M. M., Samburova, V., Hallar, A. G., Zielinska, B., Lowenthal, D. H., and Kohl, S.: Identification of water-soluble organic carbon in non-urban aerosols using ultrahigh-resolution FT-ICR mass spectrometry: organic anions, *Environ. Chem.*, 9, 285–297, doi:10.1071/EN11167, 2012.
- Odian, G.: Principles of Polymerization, John Wiley & Sons, Hoboken, New Jersey, 2004.
- Orthous-Daunay, F. R.: Empreinte moléculaire des processus post-accrétionnels dans la matière organique des chondrites carbonées, Ph. D. thesis, Institut de Planetologie et d'Astrophysique, Université Joseph Fourier, Grenoble, France, 2011.

2940

- Pearce, E. M., Wright, C. E., and Bordoloi, B. K.: Laboratory Experiments in Polymer Synthesis and Characterization, Educational Modules for Materials Science and Engineering Project, Elsevier, USA, 1–22, 1982.
- Schuchmann, H.-P. and von Sonntag, C.: Methylperoxyl radicals: a study of the γ -radiolysis of methane in oxygenated aqueous solutions, *Z. Naturforsch. B*, 39, 217–221, 1984.
- 5 Tan, Y., Carlton, A. G., Seitzinger, S. P., and Turpin, B. J.: SOA from methylglyoxal in clouds and wet aerosols: measurement and prediction of key products, *Atmos. Environ.*, 44, 5218–5226, 2010.
- 10 Tan, Y., Lim, Y. B., Altieri, K. E., Seitzinger, S. P., and Turpin, B. J.: Mechanisms leading to oligomers and SOA through aqueous photooxidation: insights from OH radical oxidation of acetic acid and methylglyoxal, *Atmos. Chem. Phys.*, 12, 801–813, doi:10.5194/acp-12-801-2012, 2012.
- von Sonntag, C. and Schuchmann, H.-P.: Peroxyl radicals in aqueous solution, In: *Peroxyl Radicals*, edited by: Alfassi, Z. B., Wiley, Chichester, pp. 173–234, 1997.
- 15 Yadav, L. D. S.: *Organic Spectroscopy*, Kluwer Academic, Secaucus, NJ, U.S.A., 7–51, 2012.
- Zhang, X., Chen, Z. M., and Zhao, Y.: Laboratory simulation for the aqueous OH-oxidation of methyl vinyl ketone and methacrolein: significance to the in-cloud SOA production, *Atmos. Chem. Phys.*, 10, 9551–9561, doi:10.5194/acp-10-9551-2010, 2010.

2941

Table 1. Experimental conditions of OH-oxidation of MVK, and comparison with our previous work, the study by Liu et al. (2012). In all studies, all experiments were unbuffered (free pH).

Exp. name/Ref.	[MKV] ₀ (mM)	[H ₂ O ₂] ₀ (mM)	O ₂ conditions ([O ₂] ₀ μM) ^{a, b}	[O ₂] (μM) at Henry's Law equilibrium ^c	Temp. (°C)	Lamp (W)	<i>J</i> (s ⁻¹)	[HO [•]] ^d (M)	τ_{life} (min) ^e	Analysis (number of experimental repetitions)
Liu et al., 2012	20	1000	Supersaturated (1700) ^a	258	25	300	7.5×10^{-7}	8.6×10^{-15}	262	HPLC-ESI-MS
A	20	400	Supersaturated (400) ^a	258	25	1000	8.5×10^{-6}	4.3×10^{-14}	52	UPLC-ESI-MS (12) ESI-UHRMS (1) UV-spectroscopy (3) NMR-spectroscopy (1)
B	20	400	Supersaturated (580) ^a	361	9	1000	8.5×10^{-6}	4.3×10^{-14}	52	UPLC-ESI-MS (1)
C	20	400	Supersaturated (656) ^a	399	5	1000	8.5×10^{-6}	4.3×10^{-14}	52	UPLC-ESI-MS (4)
D	20	400	Low (60) ^b	258	25	1000	8.5×10^{-6}	4.3×10^{-14}	52	UPLC-ESI-MS (4)
E	2	40	Supersaturated (320) ^a	258	25	1000	8.5×10^{-6}	4.3×10^{-14}	52	UPLC-ESI-MS (2) UV-spectroscopy (1)
F	0.2	4	Supersaturated (280) ^a	258	25	1000	8.5×10^{-6}	4.3×10^{-14}	52	UPLC-ESI-MS (2) UV-spectroscopy (1)

^a Dissolved O₂ concentration at time 0 (i.e. MVK introduction), in presence of H₂O₂, surrounded by ambient air; ^b dissolved O₂ concentration at time 0, in presence of H₂O₂, after 30 min of argon flow bubbling into the solution; ^c theoretical [O₂] (μM) at Henry's Law equilibrium in ambient air before H₂O₂ addition from Benson and Krause (1984); ^d the HO[•] concentrations were calculated assuming the steady state approximation at time 0: $[\text{OH}] = \frac{2 \times J \times [\text{H}_2\text{O}_2]}{k_{\text{MVK}} \times [\text{MVK}] + k_2 \times [\text{H}_2\text{O}_2]}$; ^e MVK life time towards OH-oxidation: $\tau_{\text{life}} = \frac{1}{k_{\text{MVK}}[\text{OH}]}$.

2942

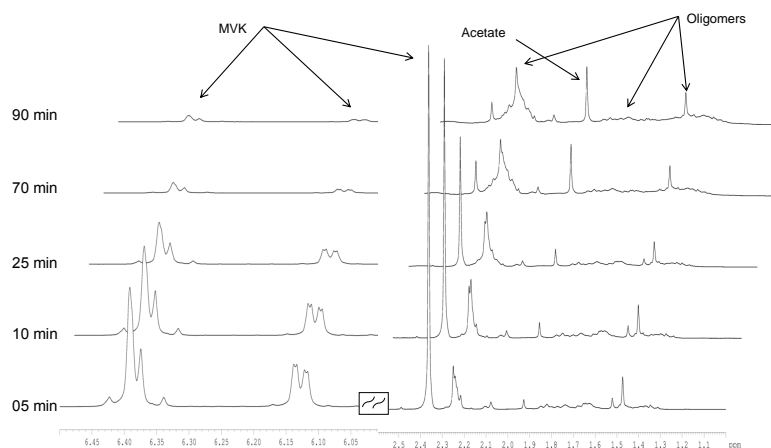


Fig. 2. Monitoring experiment A by 1-D ^1H NMR (recorded in phosphate buffer containing 10 % D_2O). The intensities of oligomer structures increase with time, to the detriment of MVK.

2945

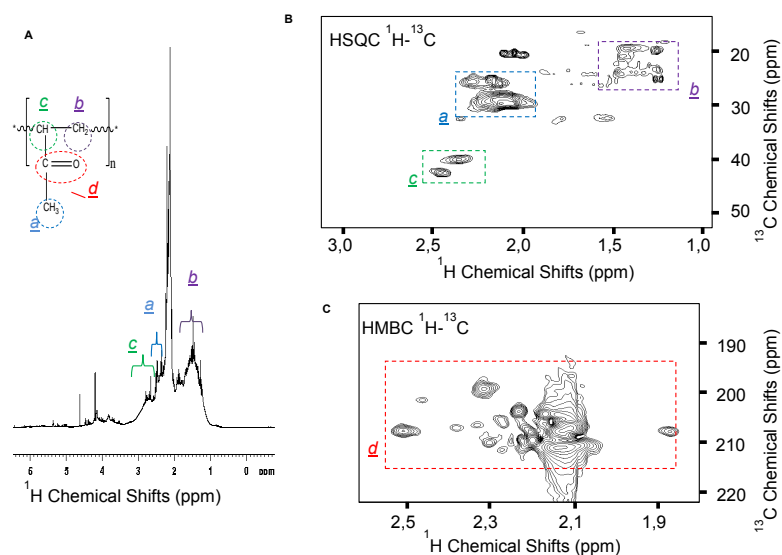


Fig. 3. Proposed structure identification of oligomers. 1-D ^1H NMR spectrum (A) and 2-D ^1H - ^{13}C NMR spectra (B and C) of a sample taken at 90 min of reaction during experiment A, freeze-dried and re-suspended in CDCl_3 .

2946

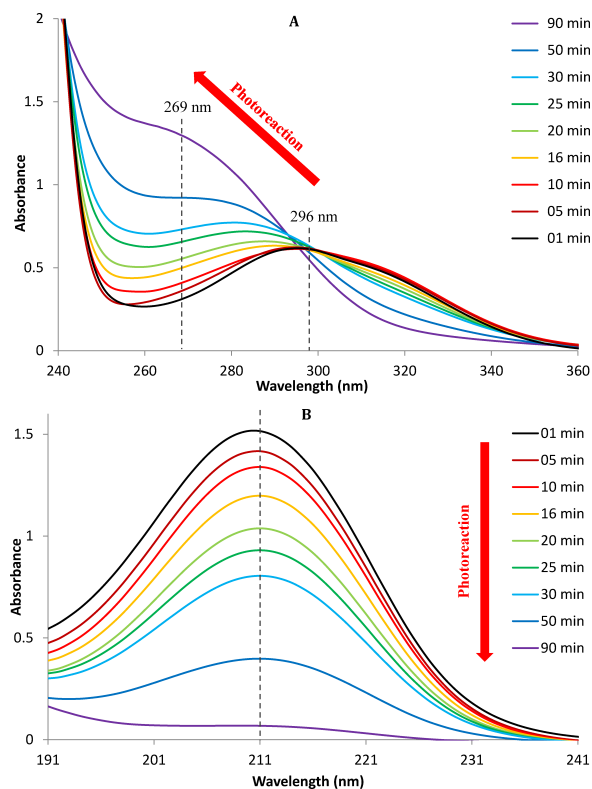


Fig. 4. UV absorption spectra of the solutions sampled during experiment A (with catalase added prior to analysis), **(A)**: from 240 to 360 nm; and **(B)**: diluted by 100 from 191 to 241 nm.

2947

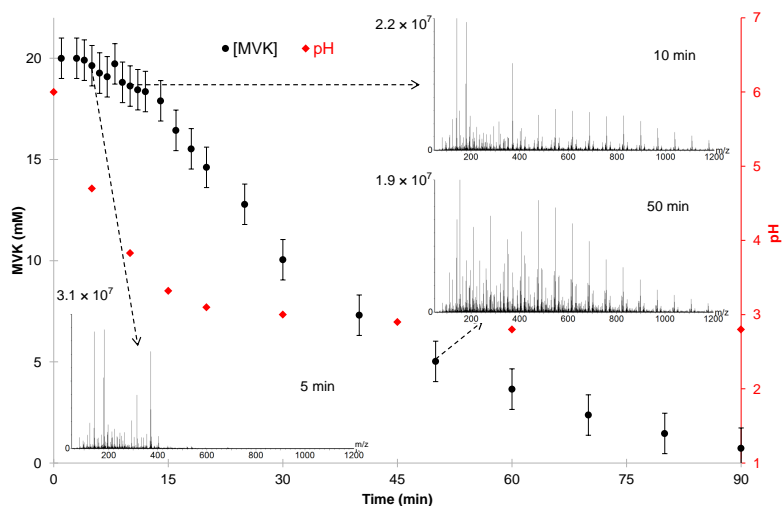


Fig. 5. MVK time profile (as measured by UV Spectroscopy) and mass spectra (obtained using UPLC-ESI-MS for the retention time range 0–5 min in the positive mode) at 5, 10 and 50 min of reaction, during experiment A (MVK 20 mM, 25 °C, under supersaturated O₂ initial conditions).

2948

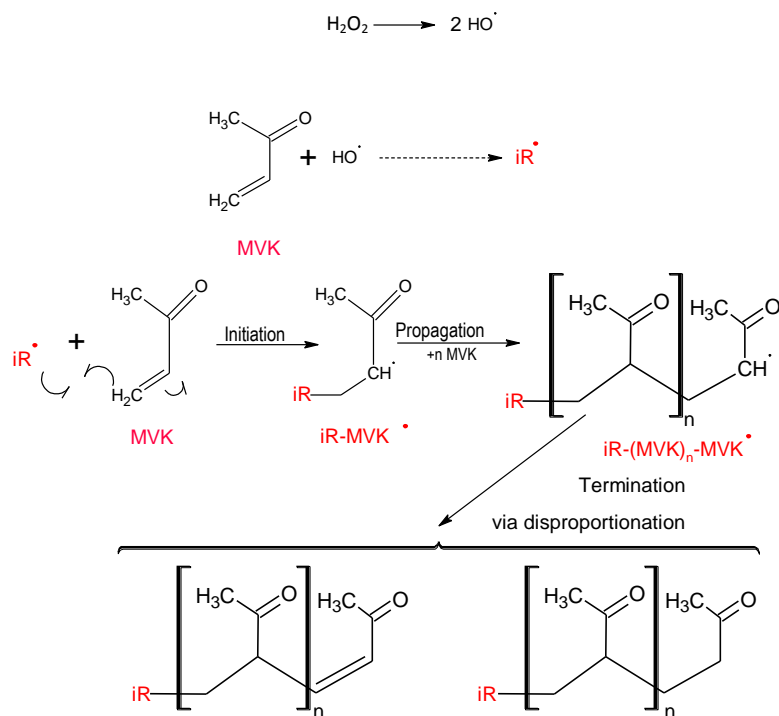


Fig. 6. Scheme of the proposed mechanism of radical oligomerization of MVK in the aqueous phase, initiated by OH-oxidation. iR^\bullet is an initiator Radical; MVK is the monomer or the repeating unit, n is the degree of polymerization. For clarity, only the external radical additions are shown.

2949

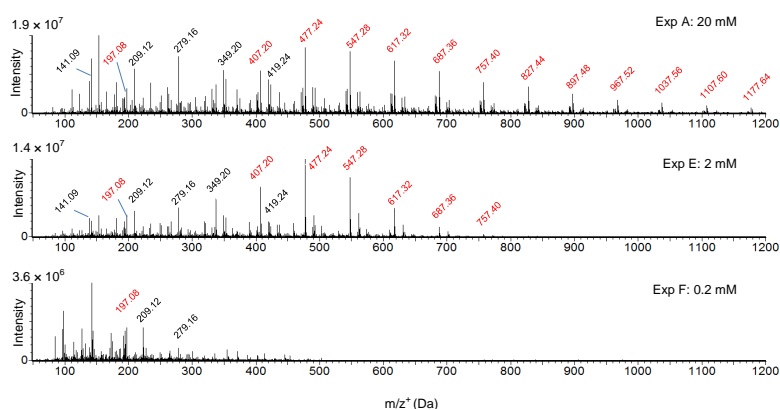


Fig. 7. Mass spectra (obtained using UPLC-ESI-MS, for the retention time range 0–5 min, in the positive mode) during experiments A, E and F (i.e. at 25 °C, for different initial MVK concentrations and at different reaction times (corresponding to the maximum oligomers intensity): 5 min for 0.2 mM; 15 min for 2 mM and 50 min for 20 mM). The most intense series (S174) is highlighted in red, as in Fig. 1).

2950

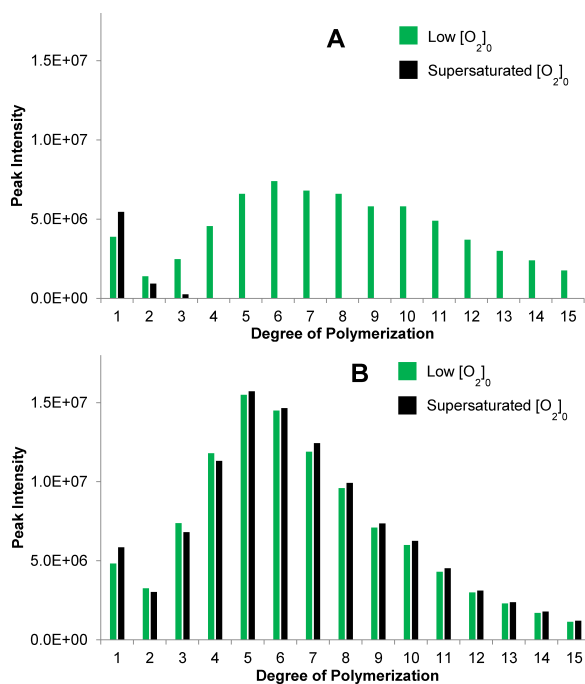


Fig. 8. Effect of initial O_2 concentrations on the oligomer series S174 up to 1200 Da (obtained using UPLC-ESI-MS, for the retention time range 0–5 min, in the positive mode) after (A) 5 min and (B) 50 min of OH-oxidation of MVK in the aqueous phase at 25 °C, under initial low O_2 conditions (in green: $[O_2]_0 = 60 \mu\text{M}$), and under initial supersaturated O_2 conditions (in black: $[O_2]_0 = 400 \mu\text{M}$).

2951

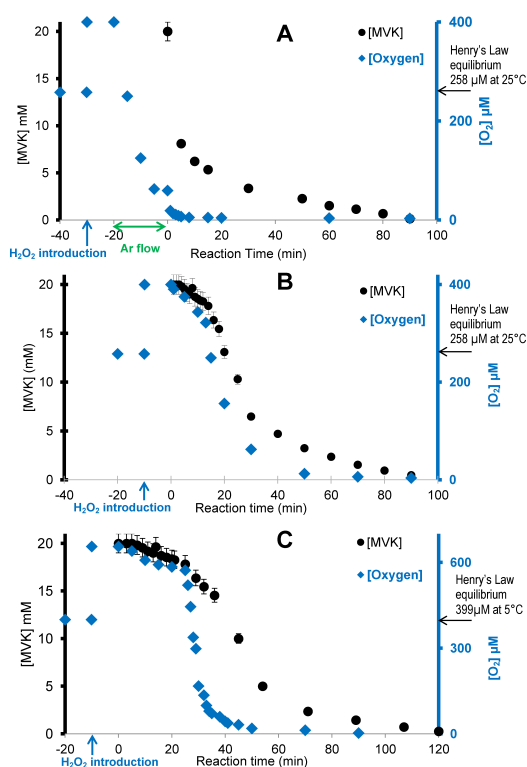


Fig. 9. Time profile of MVK and dissolved O_2 concentrations under different temperature and initial O_2 concentrations: (A) experiment D (25 °C, under low initial O_2 concentration: 60 μM); (B) experiment A (25 °C, under supersaturated initial O_2 concentration: 400 μM); (C) experiment C (5 °C, under supersaturated initial O_2 concentration: 400 μM). Time 0 = MVK introduction.

2952

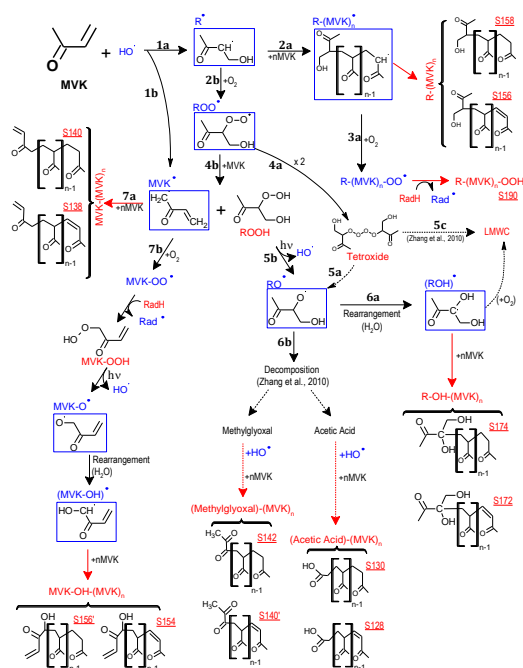


Fig. 10. Proposed scheme of the chemical mechanism of OH-oxidation of MVK in the aqueous phase with implementation of radical oligomerization pathways (for clarity, only external OH-addition on MVK is developed). RadH = MVK, HO₂ or molecular reaction products (in red). Radicals (in blue). LMWC: low-molecular-weight compounds.

2953

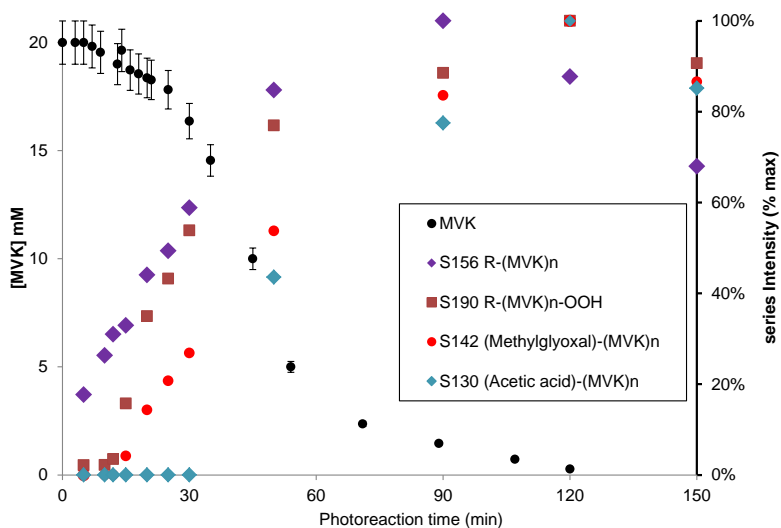


Fig. 11. MVK kinetics and Time profile of main oligomers series (obtained using UPLC-ESI-MS, for the retention time range 0–7 min, in both modes) at 5 °C. The series intensity is the sum of the peaks intensity. Each series intensity is expressed as a percentage of its maximum.

2954